Aberystwyth University

Rapid geomorphological and sedimentological changes at a modern Alpine ice margin

Le Heron, Daniel Paul; Kettler, Christoph; Davies, Bethan J.; Scharfenberg, Lars; Eder, Lukas; Ketterman, Michael; Griesmeier, Gerit E.U.; Quinn, Rhiannon; Chen, Xiaoshuai; Vandyk, Thomas; Busfield, Marie E.

Rapid geomorphological and sedimentological changes at a modern Alpine ice margin: lessons from the Gepatsch Glacier, Tirol, Austria

Daniel Paul Le Heron[1]*, Christoph Kettler[1], Bethan J. Davies[2], Lars Scharfenberg[1], Lukas Eder[1], Michael Ketterman[1], Gerit E.U. Griesmeier[3], Rhiannon Quinn[2], Xiaoshuai Chen[4], Thomas Vandyk[2] and Marie E. Busfield[5]

[1] Department of Geology, Althanstraße 14, University of Vienna, 1090 Vienna, Austria
[2] Department of Geography, Royal Holloway University of London, Surrey TW20 0EX, UK
[3] Geological Survey, Neulinggasse 38, 1030 Vienna, Austria
[4] Institute of Geology, Chinese Academy of Geological Sciences, No. 26 Baiwanzhuang Street, 100037 Beijing, China
[5] Department of Geography and Earth Sciences, Aberystwyth University, Llandinam Building, Penglais Campus, Aberystwyth SY23 3DB, UK

DPL, 0000-0002-7213-5874; CK, 0000-0003-2398-1676; LS, 0000-0003-1095-453X; TV, 0000-0002-7732-9977
* Correspondence: daniel.le-heron@univie.ac.at

Abstract: The Gepatsch Glacier in Tirol (Austria) is a rapidly retreating valley glacier whose host valley and forefield reveal subglacial, proglacial, and reworked sediment–landform assemblages. Structures include roches moutonées develop on gneiss, compound bedrock-sediment bedforms (crag and tail structures), flutes, and small diamicton ridges. The glacial sediments and landforms are undergoing incision and terrace development by meltwater streams. Glacial geomorphological and surface geological maps, in concert with elevation models of difference between July 2019 and July 2020 highlight considerable changes to the forefield over a 12-month time period. Till exposed within the last 20 years has undergone substantial mass wasting and re-deposition as subaerial mass flows, or reworked into stream deposits. The lee sides of many roches moutonées completely lack subglacial sediment, and instead contain a sand and gravel deposit interpreted to result from glaciofluvial deposition. Thus, insights into the rates of erosion and deposition in a complex, proglacial setting, allow some of these processes to be quantified for the first time. Repeated monitoring of glacier forefields is expected to yield a better understanding of the preservation potential of proglacial sedimentary facies, and hence their preservation potential in Earth's sedimentary record.

In the context of accelerating global mass loss of glaciers (Hugonnet *et al.* 2021), and amongst dismal predictions that two thirds of glacial ice in the European Alps will have disappeared by 2100 (Zekollari *et al.* 2019), intense efforts to understand the dynamics, melt behaviour, erosion processes and processes of sediment generation are underway. The demise of temperate valley glaciers has major social and environmental implications through the loss of water towers providing storage to communities further down-valley (Immerzeel *et al.* 2020) to the looming hazard of detached or collapsed glacier margins initiating catastrophic floods (Veh *et al.* 2020). Studying the paraglacial changes in the land system as the glacier retreats and the resultant imprint on the landscape is also vital for understanding the record of glaciation on Earth over geological timescales, since the first major glaciation at *c.* 2.2 Ga in the Siderian (Eyles 2008). This is because owing to the deeply carved nature of some palaeovalleys, sediments deposited within them by ancient glaciers can survive vast periods of geological time, despite the low odds of preservation. One extensively developed group of incisions are tunnel valleys, generated by large meltwater events beneath extensive ice sheets (e.g. Van der Vegt *et al.* 2012). However, on a smaller scale, bedrock valley systems allied to Alpine-style valley glaciers terminating in fjords are also widespread in the Late Paleozoic Ice Age (LPIA) record, such as in the

Paganzo Basin of Argentina (Dykstra *et al.* 2006) and in the Kaokoland uplands of northern Namibia (Dietrich *et al.* 2021).

In glacial sedimentology, it is commonly supposed that Alpine glacial environments are characterized by dramatic lateral and vertical changes in lithofacies, reflecting the competing influence of subglacial, ice-marginal and glaciofluvial processes. The latter includes cannibalization of sediment by meltwater, which has long been suspected to occur rapidly (Rose 1991). However, attempts to quantify this process are limited in Austrian Alpine environments. However, investigations of the paraglacial reworking of till have identified ground surface lowering of 2.5–4.7 m and reduction of slope gradients by 5° since about 1930 in Fåbergstølsdalen, Norway (Ballantyne and Benn 1994). In Iceland, Boulton and Dent (1974) revealed that inherent compositional factors (e.g. whether till is dilatant and sheared or compact and unsheared) are important in the post-depositional evolution of glaciogenic sediments.

In this paper, we illustrate the processes operating in the forefield of the Gepatsch Glacier, Tirol, Austria, evaluating the changes that occur in terms of sediment accumulation and erosion over a 12-month period between July 2019 and July 2020. We summarize and briefly interpret the geomorphology and sedimentology, and present geological maps of the forefield from these two snapshots in time, allowing the sedimentological and geomorphological changes. We

present the altitude difference between the two digital elevation models to quantify the rates of change in terms of deposition, cannibalization, and erosion.

Study area and previous research

The Gepatsch Glacier is a temperate valley glacier that is located at the head of the Kaunertal in the Ötztal Alps (Fig. 1), and its meltwater feeds the Fagge River. Between 1971 and 1990, the glacier lost *c.* 0.9% of its volume and retreated 1 km, according to analysis by Keutterling and Thomas (2006). This is consistent with a wider pattern of glacier retreat and thinning in Austria since the Little Ice Age (LIA) maximum in 1851, with Austrian glaciers shrinking to 44% of their LIA extent by 2004–12 (Fischer *et al.* 2015). Over the past 15 years, the Gepatsch Glacier margin has retreated a further *c.* 1 km (Fig. 1). Glacier mass loss and thinning is well expressed in the geomorphology *c.* 400 m upslope of the 2020 glacier margin, where the towering LIA lateral moraines loom over the glacier tongue (Fig. 2a). These abut against bedrock consisting of a heterogenous suite of orthogneiss, paragneiss and amphibolite. Gepatsch Glacier is clean with limited supraglacial debris cover, apart from isolated talus cones (Fig. 2b). In terms of sediment–landform assemblages, considerable attention has been given to aspects of rockfalls and slides in the Kaunertal area, both as a natural hazard as well as an important flux of sediment. Heckmann *et al.* (2016) estimated the rockfall sediment budget by integrating geomorphological mapping and fieldwork with a stochastic modelling approach over a wide area of the upper Kaunertal. The same team also delivered a very detailed assessment of large individual rockfall geomorphology, including elevation changes and the observation of a significant flux of material to the supraglacial area via rockslides. Baewert and Morche (2014) monitored sediment transport, discharge and reworking of paraglacial and proglacial sediments in Kaunertal, focusing their study on the modern river bed several kilometres downstream of the 2006 ice margin, and particularly on a heavy rainfall event in August 2012. Including very detailed terrestrial laser scanning, their aim was to quantify the role that the river bars played in sediment storage. The applied aspect to this research lies in the occurrence of a large dam, *c.* 5 km from the modern ice margin, and the importance of quantifying how quickly the dam will silt up.

There is currently little information available on the processes of glacial deposition and reworking at the modern Gepatsch Glacier ice margin. Morche *et al.* (2014) focused on sediment transport, discharge and reworking of sediments in Kaunertal, but restricted their study to the modern river bed several kilometres downtract of the 2006 ice margin. Indeed, few attempts have been made to quantify the pace of change in terms of sediment deposition and removal at modern valley glacier margins. This study addresses this, using the Gepatsch Glacier margin as a case study in sediment survival in the forefield of a narrow Alpine glacier, drawing connections between sediment preservation in the modern and deep time records.
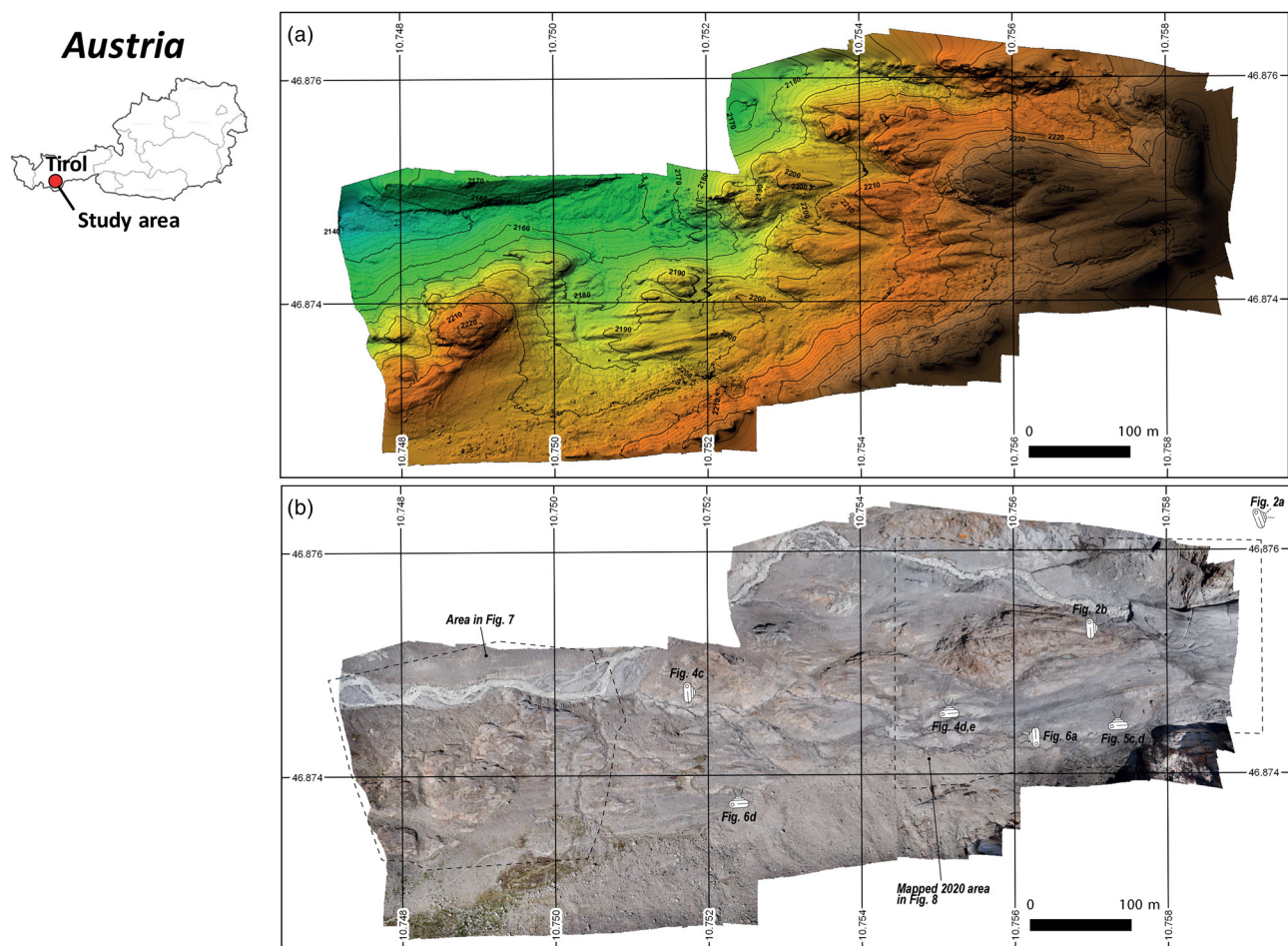
Fig. 1. (**a**) Contoured digital elevation model of the Gepatschferner/Gepatsch Glacier forefield, with inset map showing the location in Tirol, Austria. (**b**) Orthophoto mosaic image of the same area in a produced from July 2020 drone photographs. The Gepatsch Glacier itself is visible to the right of the image. The dotted outlines correspond to areas shown in more detail in Figures 7 and 8. The small camera symbols indicate the position and orientation of most of the photographs taken in this paper.

Fig. 2. General aspects of the Gepatch Glacier at the present day (2019–20). (**a**) View looking down on the glacier, *c.* 400 m from the 2020 margin, from the position of the 1851 lateral moraine ridge. In the midground, a talus cone has developed on the surface of the glacier. (**b**) View of the ice margin, showing well developed roches moutonées carved into gneiss, and the main tributary of the Fagge river to the left. The latter image was taken in July 2020.

Methods

Field data were gathered in July 2019 and exactly one year later in July 2020, including traditional sedimentological approaches (logging, facies analysis), dovetailed with photogrammetry. Geological–geomorphological maps for the glacier forefields in July 2019 and 2020 were produced following best practice (Chandler *et al.* 2018; James *et al.* 2019) and using drone imagery as a basemap. The aerial photographs were obtained using a DJI Mavic Pro quadcopter, with the inbuilt FC220 camera. This aircraft has a 1/2.3′ (CMOS) sensor capable of taking photographs of 12.35 M pixels at a focal length of 26 mm. Photos in JPEG format were taken with a maximum size of 4000 × 3000. The aircraft was automatically deployed using PIX4D Capture on an Android tablet, which was programmed to run a series of automated double grid missions with 60% image overlap. Some 1203 aerial photographs were collected in 2019, and 825 over the same area exactly 12 months later in 2020 (Supplementary material, Table 1) using ground control points. For both years, the drone was launched from the crest of a prominent crag and tail structure in the glacier forefield and commenced its grid mission at 50 m above ground level from the launch point. Five ground control points (GPCs) were drawn onto bedrock using marker pens, to remove the problem of cardboard ground control points blowing away in the wind. The data were manipulated in Agisoft Metashape Professional (Version 1.5.1

build 7618). The automated workflow was as follows, with 'high accuracy' results selected at each stage, as permitted by an 8 core workstation. Photos were aligned with key point limit of 40 000 and a tie point limit of 4000. A manual quality control check of photos was performed, and photographs with a threshold quality of <0.8 in Metashape were discarded. Thereafter, a dense point cloud (high accuracy), followed by a mesh (high face count), texture and tiled model were produced. In the final steps of processing, orthophoto mosaics (orthomosaics) and digital elevation models (DEMs) were produced and georeferenced to the WGS 84 co-ordinate system (see Supplementary material, Tables 1 and 2 for precision data and GPC positions). The orthomosaics have a resolution of 1.8 cm/pixel (2019) and 2.4 cm/pixel (2020) (Supplementary Material, Table 1). Owing to the regional slope (i.e. where the ground falls away) resolution is slightly greater at the glacier margin and decreases away from it. The DEMs have a resolution of 3.59 cm pixel^{-1} (2019) and 4.83 cm pixel^{-1} (2020). The orthomosaics were layered over the DEMs in QGIS, and a transparency algorithm applied following the methodology of Le Heron *et al.* (2019), to provide the basis for geological mapping.

Calculation of the spatial difference between the two dense clouds was completed in CloudCompare 2.11.3. To acquire smooth and accurate point clouds, an initial statistical outlier removal with 6 points for estimating mean distance was applied to both point clouds. Cropping both cleaned point clouds to the same dimensions
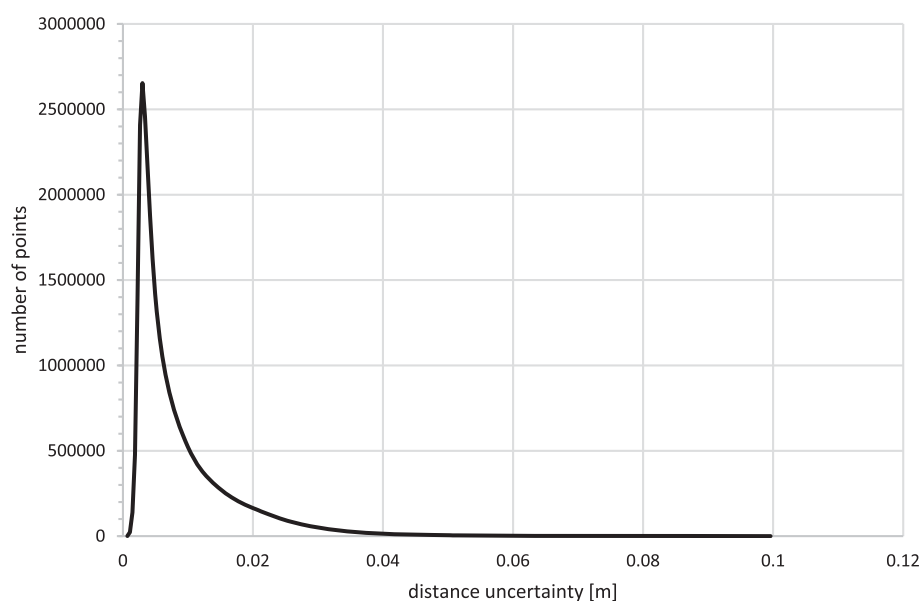
Fig. 3. Distance uncertainty for all scalar values calculated in the M3C2 algorithm. Note that peak uncertainty lies within a range of 0.001–0.02 m for 34.7 M points out of 38.2 M points.

and picking 15 reference point pairs on bedrock (e.g. joints, fractures) for both point clouds, enabled approximate alignment. Fine registering of both point clouds was secured by setting the parameters for iterations to 40 and final overlap to 90% in the built in alignment tool. Automatic adjustment of scale was unchecked to avoid distortion errors. The M3C2 algorithm (James *et al.* 2017) was applied to both point clouds to calculate significant spatial differences, allowing lateral patterns of erosion v. sedimentation to be proxied. This algorithm plots the distance between points within a certain volume from a reference point cloud (2019 record) as a scalar field onto an aligned point cloud (2020 record). In our study we used the default settings for adjustable parameters with the exception of a preferred distance calculation for the z-axis (vertical changes in elevation). Finally, scalar values are colour coded, highlighting gain or loss on the aligned point cloud. Error estimation is calculated simultaneously and given in Figure 3 as a distance uncertainty plot.

Data description

Outcrop sedimentology and geomorphology

The Gepatsch Glacier margin and its forefield is divisible into three distinct sediment–landform assemblages, in which we identify (i) a ice-contact assemblage, (ii) a glaciofluvial assemblage and (iii) a reworked assemblage. The ice-contact assemblage comprises streamlined bedrock surfaces, together with diamicton that is moulded into distinct landforms. The streamlined bedrock surfaces are particularly well exposed at the 1908 ice margin position (Fig. 4a) where p-forms, together with well-preserved striations are crosscut by quarried bedrock fractures oriented normal to palaeo-ice flow. In the lee of the bedrock fractures, gravelly sand is found (Fig. 4b). Gravelly sand is found in the lee of bedrock fractures and many roches moutonnées, including examples of the latter exposed much more recently in 2006 (Fig. 4c) and 2015 (Figs. 4d, e). Striations are best preserved where the bedrock surfaces are coated by a thin veneer of polish (Fig. 4a).

A second suite of features is recognized in the ice-contact assemblage. Small diamicton ridges occurred at the July 2020 glacier margin (Fig. 5a) measuring several metres long, approximately one-metre-wide, and about 30 cm high. The small moraines comprise muddy clast-rich diamicton dominated by sub-rounded to rounded pebble to cobble-sized clasts (Fig. 5b). Excavation revealed no structure or lithological variation within the diamicton ridges. Small flutes (6–8 m long, 30 cm high, 30 cm wide) are well

developed in an ice-flow parallel direction and are crosscut by the small diamicton ridges (Fig. 5a). Larger flutes (up to 100 m long, 3–4 m wide, up to 50 cm high) are particularly well developed at the central part of the proglacial area. Some 100 m from the 2020 glacier margin, they are also preserved as the down-ice component of crag and tail structures (Fig. 5c). The crag and tail structures measure >10 m long in a down glacier direction and attain an amplitude of several metres (Fig. 5c, d).

The glaciofluvial assemblage dominates the proglacial area, and dissects the ice-contact assemblage (Fig. 6c). Fluvioglacial gravelly sand cuts into the ice-contact assemblage and forms an accumulation *c.* 2 m thick at the banks of the modern stream. This has been progressively dissected to develop metre-scale terraces (Figs 5d, 6a, c), but also centimetre-scale terraces (Fig. 6b). Stacked, low angle trough cross-bedded sands are the dominant sedimentary facies. Pebble- to cobble sized clasts are scattered within the cross-beds, and are well represented as clast trains (Fig. 6c). The glaciofluvial environment also exhibits ephemeral features, including an ice-cored moraine (*sensu* Lukas 2011) mantled by fluvioglacial sands which was observed in 2019 (Fig. 6d). The latter deposits comprised a jigsaw puzzle-like network of highly deformed, desiccated, current ripple cross-laminated sand beds (Fig. 6e). Reappraisal of the same deposits 12 months later allowed the jigsaw puzzle-like structure to be recognized, but evidence of the rippled surfaces had been eradicated (Fig. 6f).

The reworked sediment–landform assemblage consists of two sub-assemblages reflecting their occurrence at the foot of high (>45°) and lower (<45°) slope gradients. In the presence of high slope gradients, talus cones both accumulate on the surface of the glacier (Fig. 2a) and downlap onto the glaciofluvial assemblage (Fig. 6a, c). Along lower slope gradients, runnels and gulleys dissect fluted terrain that was exposed in 2006 (Fig. 7). The runnels and gulleys radiate from an upslope feeder channel, producing a fan-shaped structure consisting of refluxed diamicton (Fig. 7).

Glacial geomorphological and surface geological maps

We have produced two geological–geomorphological maps for the July 2019 and the July 2020 glacier forefield (Fig. 8a, b). Within this twelve-month period, both the mid-channel bars and channels occupy different positions and orientations in the glaciofluvial assemblage. This is pronounced within the reaches of the main Fagge River tributary at the north of the study area, and less pronounced to the south within the tract of the smaller meltwater
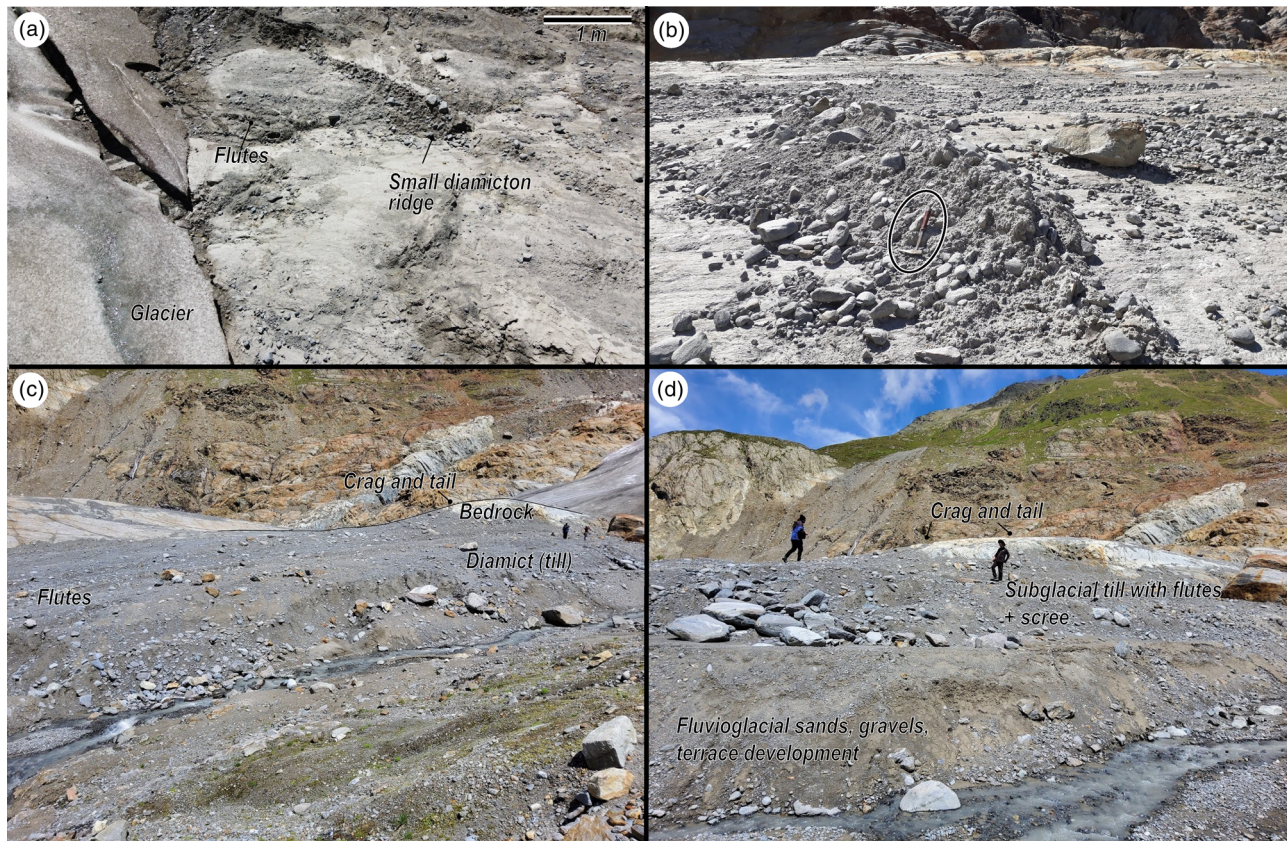
Fig. 4. Images of the subglacial sediment–landform assemblage. (**a**) Aerial view of the glacier margin and its immediate forefield, showing a glacier-margin parallel crevasse and a small annual moraine in the forefield. (**b**) Detail of the annual moraine, which consists largely of subglacial diamictons with a surface veneer of angular, supraglacial debris. In the background, flow parallel flutes and a low profile crag and tail structure can be seen imaged in (c) and (d). Looking south. (**c**, **d**) Images of a till blanket, moulded into flutes, and a crag and tail structure. Both images taken looking NE, with photo (c) somewhat further from the ice margin. All photographs (a–d) taken in July 2020.

stream. With respect to the subglacial sediment–landform assemblage, the ice margin in 2019 reveals no mappable small moraines, whereas the ice margin of 2020 reveals 5 examples of these together with the appearance of well-developed flutes (Fig. 8b). Many of the small moraines are exactly parallel to or continue into crevasses (Fig. 8b), and crosscut the flutes at the ice margin. Regions dominated by flutes in 2019, and by diamicton in general, are mapped identically in the 2020 data. However, the appearance of large boulders as scree in the glacier forefield adjacent to steep mountain slopes in the south is notable on the 2020 map: the boulders are not present on the 2019 map.

Elevation and volumetric changes in the glacier forefield (2019–20)

An image-interpretation pair enables the elevation difference between the digital elevation models produced from the drone data in 2019 and 2020 to be evaluated (Fig. 9). In these data, blue and green colours record an elevation gain, whereas pink colours record elevation loss over the twelve-month period. Substantial elevation loss on the Gepatsch Glacier on the order of several metres is allied to ablation, explaining why the margin appears as a dark pink colour on the map. Moderate elevation loss in the forefield, of the order of approximately a metre, is observed to occur to the north and in the south of the study area, in the vicinity of the Fagge River tributary and the small meltwater channel respectively. Possible slight elevation loss, of the order of decimetres, also occurs between the fluted region and the large roche moutonée (designated RM in Fig. 9), whereby 'digit-like' zones of elevation loss, each measuring up to 10 m wide, are observed. In the latter case elevation loss is

<0.2 m, which is on the limit of detection once precision and accuracy are taken into account (Chandler *et al.* 2020). The southeastern corner of the dataset shows spurious values that are interpreted as data noise. The study area also shows discrete zones of elevation gain over the same time period. These are notably developed in the main proglacial river system to the north, and evident to a lesser extent to the SW in the vicinity of the smaller meltwater stream. An extensive, 100 m wide and 50 m wide zone of elevation gain is observed to the south immediately to the east of the large zone of elevation loss (labelled 'dammed fluvial deposits' on Fig. 9). Individual blocks and boulders occur immediately to the north of the latter large zone of elevation loss and to the south of the fluted diamicton (labelled 'Talus deposits' on Fig. 9).

Interpretation

The classic polished surfaces with p-forms (Fig. 5) evidence an abundance of subglacial meltwater during the generation of roches moutonées (Sharpe 1991), an interpretation consistent with the rapid retreat patterns witnessed over the past 200 years (Fischer *et al.* 2015). With regard to sediment-cored landforms, ice marginal moraines can accumulate on a very short (annual to sub-annual) timescale. For example, Chandler *et al.* (2020) mapped spatially complex, saw tooth patterns in the forefield of the modern Fjallsjökull piedmont glacier in Iceland. There, small 'squeeze' moraines were proposed to originate during meltwater-driven events and larger push moraines during winter re-advances. Similarly, at Schwarzensteinkees in the Zillertal in Tirol, minor moraines are recognized to form by push events during ice margin oscillations (Wyshnytzky *et al.* 2020). At the Gepatsch Glacier margin, an

Fig. 5. Relationships between subglacially moulded landforms and overlying and adjacent sediments in the Gepatsch Glacier forefield. (**a**) Streamlined bedforms with sediment preferentially preserved in down-ice p-forms and in the lee of fractures traversing the gneiss. Aerial photograph not shown on Figure 1, but taken at 46° 52.943′N 10° 44.326′E. (**b**) Detail of the mantling sediment reveals that this is sandy gravel. (**c**) Gravelly sand preserved in the lee of a roche moutonée, exposed following retreat in 2006. (**d, e**) Roche moutonée developed on paragneiss bedrock with lee-side gravelly sand, exposed in 2012. All photos taken in July 2020.

important observation is that the small diamicton ridges are oriented parallel to the crevasses. Thus, rather than englacial thrusting, we tentatively propose that the small diamicton ridges may be interpreted as small crevasse squeeze ridges or infills.

The flutes on the Gepatsch Glacier forefield show characteristics of those found at temperate ice margins (e.g. Ely *et al.* 2018). Flutes tend to form in the lee of initiating boulders, and some have argued that they result from a largely depositional process whereby lateral
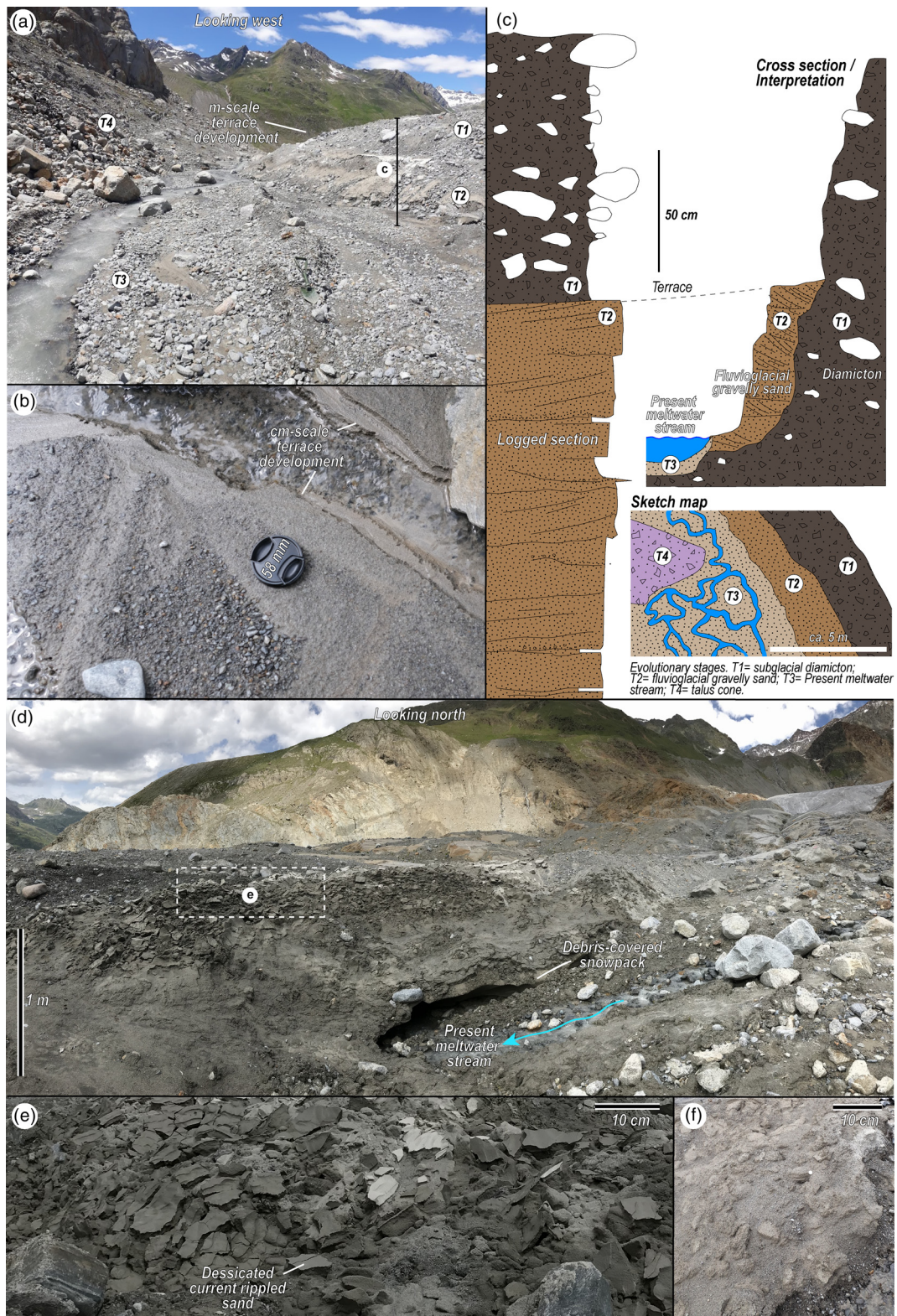
Fig. 6. The glaciofluvial assemblage. (**a**) Extant meltwater stream dissecting metre-scale terraces through diamictons and recently deposited gravelly sand. Profile and symbols T1-4 correspond to stages of evolution shown in (c). Photo taken in July 2020. (**b**) Terrace incision at the centimetre-scale, emphasizing the trend of reworking and cannibalization in the proglacial environment. Photo taken in July 2020. (**c**) Sedimentary log through the deposits shown in (a), together with an interpreted cross sectional profile and a simple sketch map showing the distribution of lithofacies in plan view in this small area. Four simple evolutionary phases are recognized to explain the observed sediment–landform assemblage. It is emphasized that all of these phases represent the time interval from 2006 to the present day. (**d**) The complexity of the glaciofluvial environment is emphasized by snowpack mantling glaciofluvial sandy gravel, upon which glaciofluvial rippled sands have been deposited and subsequently abandoned as the river dissects deeper, disappearing under the snowpack. Photo taken in July 2019. (**e**) Desiccated current-ripple cross laminated sands in July 2019. (**f**) The remains of the same cross-laminated sands in July 2020.
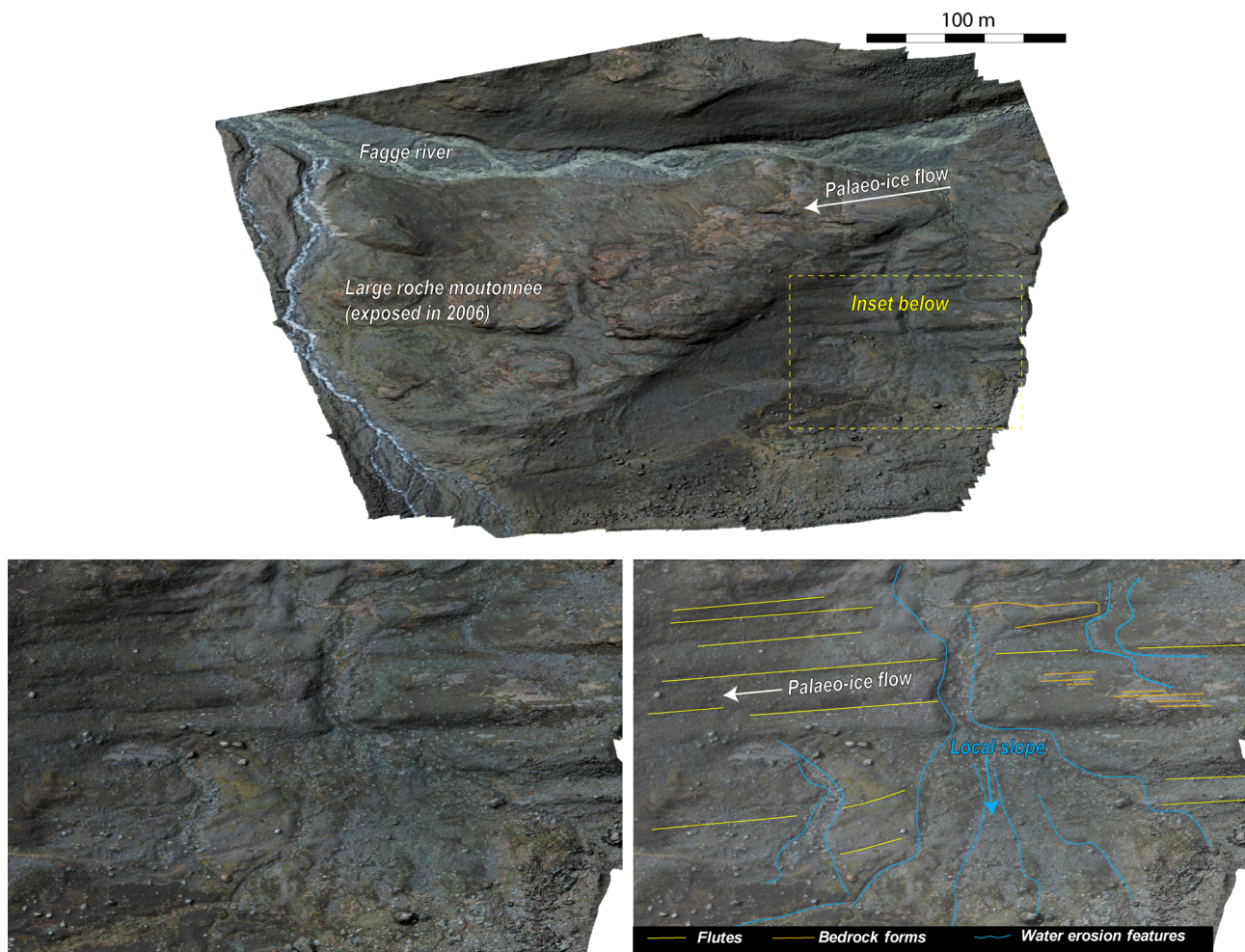
Fig. 7 Aerial view of part of the glacier forefield that was exposed in 2006, showing the relationship between the ice-contact assemblage and the reworked assemblage. The large image represents a digital elevation model (DEM) draped with a partially transparent orthophoto composite (see Methods section). Broadly speaking, the reddish areas together with the large roche moutonée comprise metamorphic bedrock, and the grey area sediment. Inset images show fluted terrain developed at the southern flank of the roche moutonée, with the interpretation of flutes, associated small scale bedrock streamlined forms, and water erosion features indicated. These latter structures constitute part of the reworked assemblage.

flow cells in basal ice transports sediment in the deformable bed out of troughs and onto ridges (Roberson *et al.* 2011). This cavity filling hypothesis has been recently supported by approaches such as till magnetic susceptibility analysis (Ives and Iverson 2019). Others have emphasized that flutes can form through a combination of erosion and deposition, throughout the year including the winter (Hart *et al.* 2018). At the Gepatsch margin, the crosscutting relationship between the flutes and the annual moraines may imply that subglacial conditions transitioned from those whereby flute formation was favoured, to those where flow-orthogonal structures (the small moraines) was promoted. The role of both depositional and erosional processes at work in the ice-contact assemblage (Hart *et al.* 2018) is recognized at a larger scale in the generation of the crag and tail structures. The smoothed, elongate bedrock ridge that constitutes the up-ice portion of our figured example (Fig. 4c, d) represents erosion, with the diamicton in the lee side representing a depositional continuation of the elongate, subglacial bedform. Thus, deposition of till in the 'pressure shadow' of the bedrock crag occurred, with the smoothed profile of the diamicton in the lee developing by subglacial moulding (Nitsche *et al.* 2016).

Crosscutting relationships enable a four-phased evolution to be recognized (Fig. 6a, c): deposition of subglacial diamicton (T1); fluvioglacial deposition and terrace incision (T2); cutting of present meltwater channel (T3); and delivery of scree via small talus cones to the proglacial area (T4). Three aspects of the glaciofluvial

assemblage require explanation, namely (i) the origin of terraces on different scales, (ii) the role of talus cone emplacement and their interference with sedimentation patterns, and (iii) the preservation potential of sediments. Put simply, terrace development records the reduction of accommodation space and the progressive incision of streams. To the south of the study area, metre-scale terrace development is interpreted to record rapid (local) base level fall within the small fluvial basin. Given the evidence for talus cones influencing the course and direction of the meltwater stream, it is proposed that failure of slope material in a similar way blocked the drainage of the small meltwater channel. Ponding and backfilling with sands and gravels occurred, until the stream system was able to erode and overcome the damming effects of the talus cone, producing a sudden local downcut. Although the timeframe of development could be reconciled with localized hinterland rejuvenation e.g. localized neotectonic uplift along a fault (Székely *et al.* 2002), all features can be adequately explained via an autocyclic mechanism. The centimetre-scale terrace development is unlikely to be related to the metre-scale terraces, and instead charts the local avulsion of individual, small streams and the incision of dm-scale mid channel bars.

In respect to the reworked assemblage, we have already considered the talus cones above. The development of runnels crosscutting the flutes (Fig. 7), however, points to a different process at work. We interpret these to reflect the channelization of rainwater
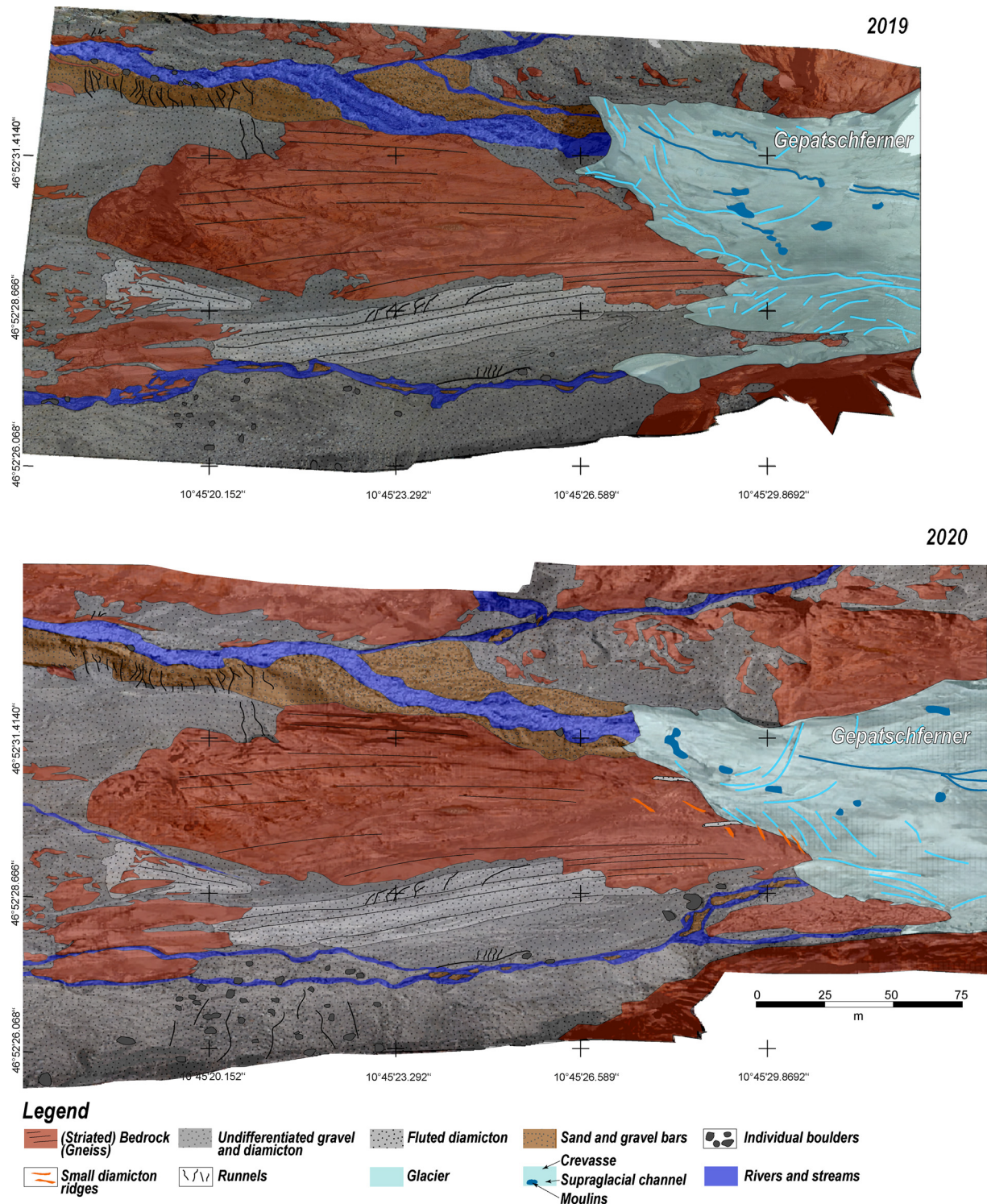
Fig. 8 Geological maps of the Gepatsch Glacier forefield for July 2019 and July 2020. In each case, the base map comprises of a DEM layered with a semi-transparent orthophoto mosaic. Notable changes over a 12-month period include the development of annual moraines and flutes at the glacier margin and the delivery of large blocks via slope collapse onto the glacier forefield.

runoff, and their orientation reflects the local (decimetre- to metre-scale) orientation of the slope. Sediment bypass and transport within the runnels promoted small-scale incision, and where the slope gradient decreased sufficiently to suppress sediment transport, a fan body was deposited (Fig. 7). As noted previously, the studied runnels were exposed in 2006. Thus, the rate of flute degradation compares to that already noted by Rose (1991). Working on the Austre Okstindbreen Glacier, Rose (1991) identified a range of processes that were responsible for the immediate reworking of flutes immediately after deposition. Gelifluction, frost heave and

surface wash considerably reworked original till fabrics, and a low 'survival potential' of small flutes was proposed. At the Gepatsch site, we emphasize the surface wash mechanism to explain the runnels and the fan. It would be expected that this refluxed till would also have lost its original subglacial fabric (Ballantyne and Benn 1994).

In map view, the changing geometry of the channels and braid bars in the main Fagge River tributary is interpreted to record channel avulsion and shifting braid-bar positions over the study interval. Although apparent when comparing the 2019 and 2020
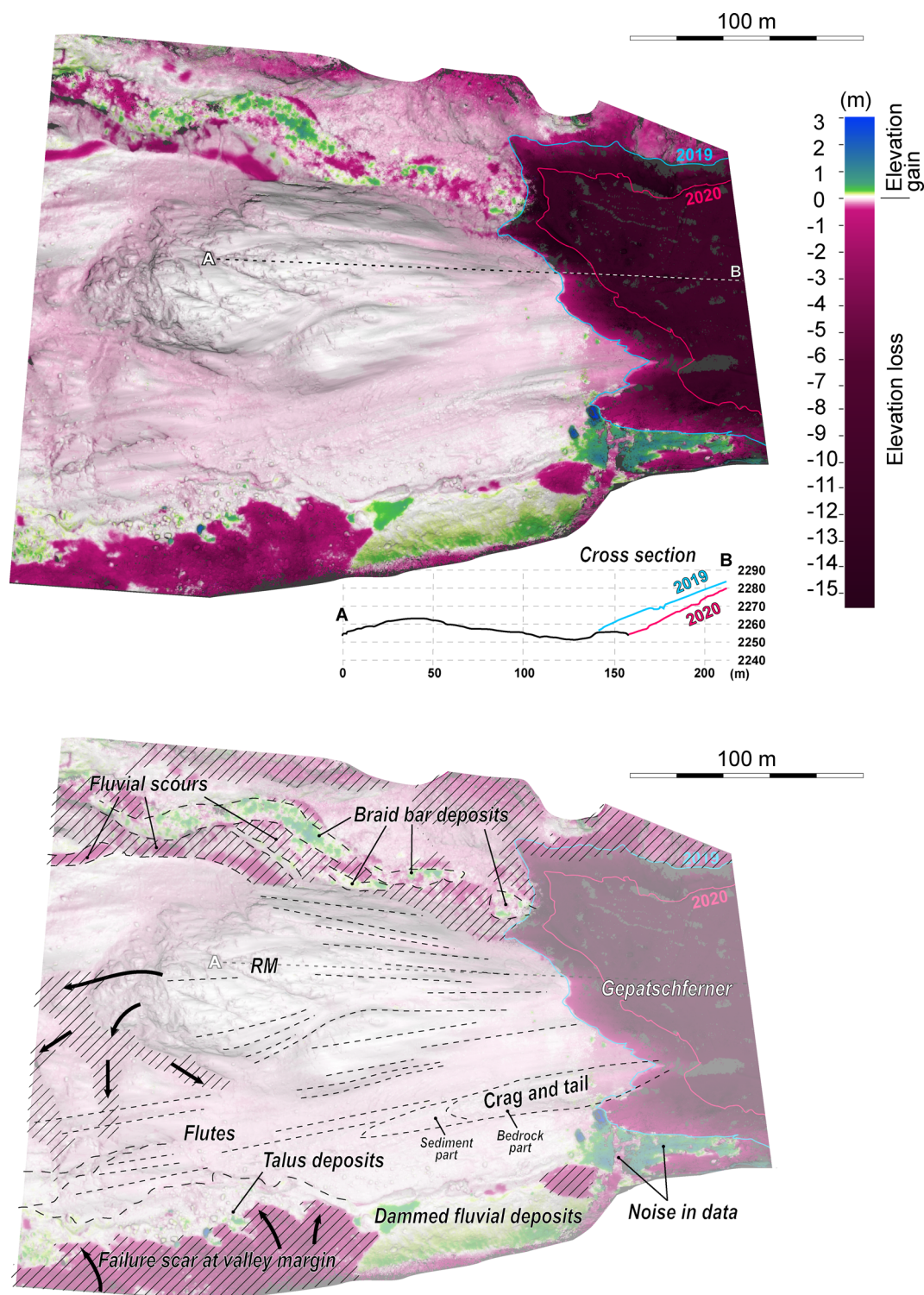
Fig. 9 CloudCompare model that shows the difference between the dense point clouds used to calculate the digital elevation models of both 2019 and 2020 vintages. The glacier is shown in a solid red colour because this experienced the greatest change over a 12-month period. Conversely, the gneiss bedrock in the glacier forefield shows zero detectable change in this interval. The flutes and proglacial sediments, meanwhile, show evidence of sediment transport (green to yellow hues) implying that these have undergone detectable cannibalization over a 12-month interval. This is in spite of the area lying between the two main meltwater conduits.

geological–geomorphological maps (Fig. 8), digital elevation model of difference data expresses these processes more clearly in terms in zones of elevation loss (interpreted as erosion) and gain (interpreted as deposition). The zones of elevation loss in the main Fagge River tributary are thus interpreted as scours produced by switching braided channel positions, whereas the zones of elevation gain in the river are interpreted as newly deposited braid bars. To the south of the study area, a different explanation is required, whereby

the large (*c.* 150 m long, 30 m wide) zone of elevation loss (Fig. 9) is interpreted to result from hillslope degradation. The digit-like zones of elevation loss between the roche moutonée and the flutes is interpreted to record a complex network of runnels (Fig. 9) analogous to those observed on aerial photographs (Fig. 7). Hillslope degradation to the south of the study area is likely to have resulted from ablation of an underlying snowpack observed in 2019 (e.g. Fig. 6d), and is interpreted to have had two major impacts

on sedimentation patterns. The first is the accumulation of a substantial zone of fluvial deposits immediately to the east of the zone of mass wasting, and the second is the development of a boulder field immediately to its north. We interpret hillslope failure to have produced talus cones, which locally dammed and ponded the meltwater channels to produce a confined basin (Fig. 9). The same failure process (rockfalls) and formation of the talus cones explains the presence of large boulders and blocks to the south of the fluted area as shown on the geological–geomorphological map of 2020 (Fig. 8). It should be noted that small moraines do not appear on the digital elevation model of difference data, because although they would be expected to record elevation gain onto a surface that was previously devoid of sediment, that same surface was covered by ice in 2019. Given the generally coarse-grained nature of the glaciofluvial assemblage, it is expected that rather energetic flows are required to dissect and ultimately position-shift the braid bars at flood water. Since our data were gathered in July in the middle of the melt season, it is proposed that these changes likely occurred in the second part of the melt season in 2019, before the winter. *c.* 2 km from the 2020 glacier margin, Morche *et al.* (2014) documented similar dynamics in the Fagge River. Individual, major rainfall events in August 2012 were shown to play a significant role in the reconfiguration of the braid bars (Baewert and Morche 2014).

At the ice margin, the appearance of the small moraines at the glacier margin in 2020 is remarkable, given their complete absence in 2019. Mapping their trend, i.e. lying approximately ice-margin and crevasse-parallel, sheds further light on the genesis of these structures in general. Many crevasses in ice frontal positions represent englacial thrusts (Phillips 2018). Limited throw on these structures, instigated through compression upglacier during the winter, can also affect immediately underlying diamicton, which is squeezed up into the cavity. Thus, in the case of the small moraines at the Gepatsch Glacier margin, envisaged processes include one or more of simple pushing and thrusting (including direct association with crevasse propagation), and subglacial freeze on and rafting (Wyshnytzky *et al.* 2020).

Discussion

Considering the interpretations resulting from field observations, geological–geomorphological mapping and digital elevation models of difference, the following changes over a 12-month period can be distilled. Firstly, within the subglacial sediment–landform assemblage, well-expressed, small diamicton ridges appeared, and flutes and crag and tail structures were increasingly exposed through ice margin retreat. Second, within the glaciofluvial assemblage, shifts in the braid bars and channels were observed. On a small scale, terrace incision continues to be expressed, and weathering of distinctive, desiccated current rippled sands was recorded. Thirdly, it has been demonstrated that the processes and products of reworking (here denoted the 'reworked assemblage') are well expressed over this time interval and include (i) talus cone formation, (ii) damming and modification of the meltwater streams, (iii) the deposition or large boulders via rockfalls from the valley margin, and (iv) reduction in elevation (and thus erosion) of flutes and diamicton in the lee of large bedrock structures. In the proglacial area, it has been shown that sandy and gravelly deposits, rather than diamicton, occurs in the lee of many roches moutonées. We interpret this to mean that fluvioglacial deposits have a greater survival potential in Kaunertal than subglacial deposits in the proglacial valley floor. The obvious exception to this is the large Little Ice Age lateral moraine complex plastered to the valley sides. Although the evolution of glacier forefields over the timescale of multiple glacial cycles in terms of sediment yield has been characterized using conceptual numerical models (e.g. Antioniazza and Lane 2021) or via source to sink approaches

(Jaeger and Koppes 2016), we argue that a classic approach embracing sedimentological and geomorphological mapping, dovetailed with digital mapping, has an important role to play in documenting change.

At Kaunertal, the glaciofluvial system appears to be highly responsive to short term changes. In their terrestrial laser scanner analysis of the Fagge River, Baewert and Morche (2014) demonstrated that significant elevation loss occurred following a heavy rain event on August 26th 2012. That study illustrated that coarse-grained sediment storage in river bars witnessed an overall accumulation downtract, but immediately in front of the glacier margin significant elevation loss occurred, including the dissection of an ice-cored moraine during the rainstorm. In contrast, over a similar time interval to that study, we have shown that detectable accumulation does occur at the glacier margin, in response to ponding of glaciofluvial sediments by newly formed talus cones. The metre-scale terrace development, with reference to the results of Baewert and Morche (2014), could thus reflect a single large rainfall event rather than progressive downcutting and incision over a longer period. A potential mechanism would be the breaching of an earlier talus 'dam' during a heavy rainfall event. Recent mapping of slope collapse processes and products affecting the valley walls further upglacier Vehling *et al.* (2017) suggests that the development of talus cones, and their subsequent erosion, is not unusual. Their mapping, underpinned by terrestrial and airborne LiDAR, detected a local surface change of up to −10 m from the so-called 'Schwarze Wand' (Fig. 2a) between summer 2012 and summer 2014. These workers also documented a single block measuring 100 m^3 was released from the rockslide scar in a single event, coming to rest on the surface of the glacier (Vehling *et al.* 2017; their fig. 6). In sedimentological terms, of interest is the immediate response of the system to accumulate significant glaciofluvial sediment, dammed by the talus cones. This may increase sediment preservation potential.

Our study has emphasized the short time frame of depositional shifts at a modern Alpine valley glacier margin. It is commonly assumed that the preservation potential of Alpine glacial deposits in the sedimentary record is very low, and more generally, that there is a stronger bias towards glaciomarine deposits in the sedimentary record because of the tendency of mountainous areas to degrade and erode over geological timescales (e.g. Eyles 1993). In spite of this, there remains excellent evidence for deeply incised, formerly glaciated landscapes, at least as far back as the Late Paleozoic Ice Age (LPIA). Many of these landscapes have close parallels with Kaunertal, and the sediment–landform assemblages at least partly comparable to those in the present-day Gepatsch Glacier forefield. For instance, the occurrence of scratched and polished surfaces along near-vertical modern day valleys in northern Namibia (Martin and Schalk 1959) locally overlain by 300 Ma old diamictites and fluvial deposits (Dietrich *et al.* 2021), represent a classic example. In the Paganzo Basin of Argentina, slightly older diamictites adorn the bases of gorge-like incisions that were interpreted as palaeofjords (Tedesco *et al.* 2016). Furthermore, deep bedrock incisions bearing striation and overlain by glaciofluvial sediments, also produced during the LPIA, are reported from the Parana Basin of Brazil (Fallgatter and Paim 2019). In even older (700 Ma) rocks, up to 30 m deep palaeovalleys occur in Mirbat, southern Oman, which were cut during the Cryogenian and draped with an initial fill of glaciofluvial sands and gravels (Rieu *et al.* 2006). Such ancient examples demand a full understanding of the preservation potential, as well as preservation biases, at work in modern upland glacial environments.

In recent years, there has been a rapid expansion of drone-based surveys and Structure from Motion photogrammetry in studies of glacial geomorphology, yet the application of this technology to glacial sedimentology is not widespread (Śledź *et al.* 2021). Instead,

much effort is invested in monitoring paraglacial slopes or rock glacier activity (Kaufmann *et al.* 2018), on deploying drones to document glacier volume loss (e.g. Cao *et al.* 2021), or specifically on the geomorphology of glacier forefields (e.g. Dąbski *et al.* 2020). Repeated surveys of other valley glaciers have resulted in landsystem-scale geomorphic maps. For example, in a 4-year series of time 'snapshots' from 2010–13, Avian *et al.* (2018) employed ground-based LiDAR surveys. This work led to a suite of excellent geomorphic maps, allowing the spatial and temporal evolution of landforms to be characterized during retreat of this glacier, albeit with little information on facies distribution. It is proposed that repeat surveys of other glacial margins, with particular focus on sedimentology as well as geomorphology, should be undertaken. In the deep time sedimentary record, glacial sediment-ary models include not only sediment–landform systems that are very reminiscent of their modern counterparts, but may include palaeo–geomorphological and sedimentological features that are difficult to interpret from individual 'snapshot' impressions that a geologist gains by visiting a glacier margin, but are better understood through repeated surveys. Such an approach is expected to feed into better sedimentary models at glacier margins, and in turn to a more realistic and reasoned interpretation of the sedimentary record.

Conclusions

- The proglacial area of the Gepatsch Glacier can be described in terms of three sediment–landform assemblages. These are an ice-contact assemblage, a glaciofluvial assemblage and a reworked assemblage. The ice-contact assemblage includes roches moutonées, crag and tail structures, flutes and small diamicton ridges. The glaciofluvial assemblage comprises sands and gravels organized into a series of metre-scale terraces. The reworked assemblage includes large-scale resedimentation features (talus cones) as well as small-scale runnels that testify to reworking of the other two assemblages;

- Integration of field observations with data derived from a drone reveal significant reorganization of the proglacial area over a 12-month period. This includes (i) talus cones developing that ponded sediment, promoting fluvial sediment deposition in a minibasin; (ii) detectable degradation of diamicton, (iii) growth of small annual moraines before July 2020, and (iv) channel bar migration in the proglacial river. Study of fluted terrain at the 2006 ice margin position illustrates significant runneling and reworking of diamicton as a minor fan deposit at the flanks of a large roche moutonée;

- Given previous studies that have documented instantaneous change owing to heavy rainfall events downtract (Baewert and Morche 2014), or instant change owing to hillslope collapse via rockfalls or slides uptract (Vehling *et al.* 2017), we emphasize the important of sudden, rather than gradual change in governing the processes operating at the Gepatsch Glacier margin. Through the lens of the rock record, these sudden changes imply that autocyclic processes may be strongly represented in the Paleozoic or Precambrian record where that record is preserved in similar, palaeo–Alpine settings.

Data availability All data generated or analysed during this study are included in this published article.

Scientific editing by Philip Hughes

References

Antoniazza, G. and Lane, S.L. 2021. Sediment yield over glacial cycles: A conceptual model. *Progress in Physical Geography*, first published online 9 March 2021, https://doi.org/10.1177/0309133321997292

Avian, M., Kellerer-Pirklbauer, A. and Lieb, G.K. 2018. Geomorphic consequences of rapid deglaciation at Pasterze Glacier, Hohe Tauern Range, Austria, between 2010 and 2013 based on repeated terrestrial laser scanning data. *Geomorphology*, **310**, 1–14, https://doi.org/10.1016/j.geomorph.2018.02.003

Baewert, H. and Morche, D. 2014. Coarse sediment dynamics in a proglacial fluvial system (Fagge River, Tyrol). *Geomorphology*, **218**, 88–97, https://doi.org/10.1016/j.geomorph.2013.10.021

Ballantyne, C.K. and Benn, D.I. 1994. Paraglacial slope adjustment and resedimentation following recent glacier retreat paraglacial slope adjustment and resedimentation following recent glacier retreat, Fåbergstølsdalen. *Arctic and Alpine Research*, **26**, 255–269, https://doi.org/10.1080/0004082003065 https://doi.org/10.2307/1551938

Boulton, G.S. and Dent, D.L. 1974. The nature and rates of post-depositional changes in recently deposited till from south-east Iceland. *Geografiska Annaler: Series A, Physical Geography*, **56**, 121–134, https://doi.org/10.1080/04353676.1974.11879894

Cao, B., Guan, W., Li, K., Pan, B. and Sun, X. 2021. High-resolution monitoring of glacier mass balance and dynamics with unmanned aerial vehicles on the Ningchan No. 1 Glacier in the Qilian Mountains, China. *Remote Sensing*, **13**, 2735, https://doi.org/10.3390/rs13142735

Chandler, B.M.P., Lovell, H. *et al.* 2018. Glacial geomorphological mapping: A review of approaches and frameworks for best practice. *Earth-Science Reviews*, **185**, 806-846, https://doi.org/10.1016/j.earscirev.2018.07.015

Chandler, B.M.P., Chandler, S.J.P. *et al.* 2020. Sub-annual moraine formation at an active temperate Icelandic glacier. *Earth Surface Processes and Landforms*, **45**, 1622–1643, https://doi.org/10.1002/esp.4835

Dąbski, M., Zmarz, A. *et al.* 2020. Mapping Glacier Forelands Based on UAV BVLOS Operation in Antarctica. *Remote Sensing*, **12**, 630, https://doi.org/10.3390/rs12040630

Dietrich, P., Griffis, N.P. *et al.* 2021. Fjords network in Namibia: A snapshot into the dynamics of the late Paleozoic Glaciation. *Geology*, **49**, https://doi.org/10.1130/G49067.1

Dykstra, M., Kneller, B. and Milana, J.P. 2006. Deglacial and postglacial sedimentary architecture in a deeply incised paleovalley-paleofjord; the late Carboniferous (Pennsylvanian) Jejenes Formation, San Juan, Argentina. *GSA Bulletin*, **118**, 913-937, https://doi.org/10.1130/B25810.1

Ely, J.C., Graham, C., Barr, L.D., Rea, B.R., Spagnolo, M. and Evans, J. 2018. Using UAV acquired photography and structure from motion techniques for studying glacier landforms: Application to the glacial flutes at Isfallsglaciaren. *Earth Surface Processes and Landforms*, **42**, 877–888, https://doi.org/10.1002/esp.4044

Eyles, N. 1993. Earth's glacial record and its tectonic setting. *Earth-Science Reviews*, **35**, 1-248, https://doi.org/10.1016/0012-8252(93)90002-O

Eyles, N. 2008. Glacio-epochs and the supercontinent cycle after *c.* 3.0 Ga: Tectonic boundary conditions for glaciation. *Palaeogeography, Palaeoclimatology, Palaeoecology*, **258**, 89–129, https://doi.org/10.1016/j.palaeo.2007.09.021

Fallgatter, C. and Paim, P.S.G. 2019. On the origin of the Itararé Group basal nonconformity and its implications for the Late Paleozoic glaciation in the Paraná Basin, Brazil. *Palaeogeography, Palaeoclimatology, Palaeoecology*, **531**, https://doi.org/10.1016/j.palaeo.2017.02.039

Fischer, A., Seiser, B., Stocker-Waldhuber, M., Mitterer, C. and Abermann, J. 2015. The Austrian Glacier Inventories GI1 (1969), GI2 (1998), GI3 (2006) and GI LIA in ArcGIS (shapefile) format. Supplement to https://doi.org/10.5194/tc-9-753-2015. *PANGAEA*, https://doi.org/10.1594/PANGAEA.844988

Hart, J.K., Clayton, A.I., Martinez, K. and Robson, B.A. 2018. Erosional and depositional subglacial streamlining processes at Skálafellsjökull, Iceland: an analogue for a new bedform continuum model. *GFF*, **140**, 153–169, https://doi.org/10.1080/11035897.2018.1477830

Heckmann, T., Hilger, L., Vehling, L. and Becht, M. 2016. Integrating field measurements, a geomorphological map and stochastic modelling to estimate the spatially distributed rockfall sediment budget of the Upper Kaunertal, Austrian Central Alps. *Geomorphology*, **260**, 16–31, https://doi.org/10.1016/j.geomorph.2015.07.003

Hugonnet, R., McNabb, R. *et al.* 2021. Accelerated global glacier mass loss in the early twenty-first century. *Nature*, **592**, 726–731, https://doi.org/10.1038/s41586-021-03436-z

Immerzeel, W., Lutz, A. *et al.* 2020. Importance and vulnerability of the world's water towers. *Nature*, **577**, 364–369, https://doi.org/10.1038/s41586-019-1822-y

Ives, L.R.W. and Iverson, N.R. 2019. Genesis of glacial flutes inferred from observations at Múlajökull, Iceland. 47, 387-390, *Geology*, https://doi.org/10.1130/G45714.1

Jaeger, J.M. and Koppes, M.N. 2016. The role of the cryosphere in source-to-sink systems. *Earth-Science Reviews*, **153**, 43–76. https://doi.org/10.1016/j.earscirev.2015.09.011.

James, R.M., Robson, S. and Smith, M.W. 2017. 3-D uncertainty-based topographic change detection with structure-from-motion photogrammetry: precision maps for ground control and directly georeferenced surveys. *Earth Surface Processes and Landforms*, **42**, https://doi.org/10.1002/esp.4125

James, M.R., Chandler, J.H. *et al.* 2019. Guidelines on the use of structure-from-motion photogrammetry in geomorphic research. *Earth Surface Processes and Landforms*, **44**, 2081–2084, https://doi.org/10.1002/esp.4637

Kaufmann, V., Seier, G., Sulzer, W., Wecht, M., Liu, Q., Lauk, G. and Maurer, M. 2018. Rock glacier monitoring using aerial photographs: conventional vs. UAV-based mapping - a comparative study. *International Archives of the Photogrammetry, Remote Sensing and Spatial Information Sciences*, **42**, 239–246, https://doi.org/10.5194/isprs-archives-XLII-1-239-2018

Keutterling, A. and Thomas, A. 2006. Monitoring glacier elevation and volume changes with digital photogrammetry and GIS at Gepatschferner glacier, Austria. *International Journal of Remote Sensing*, **27**, 4371–4380, https://doi.org/10.1080/01431160600851819

Le Heron, D.P., Vandyk, T.M. *et al.* 2019. Bird's-eye view of an Ediacaran subglacial landscape. *Geology*, **47**, 705–709, https://doi.org/10.1130/G46285.1

Lukas, S. 2011. *Ice Cored Moraines. Encyclopedia of Earth Sciences Series, Part 3, 616–618*. Springer Nature.

Martin, H. and Schalk, K. 1959. Gletscherschliffe an der Wand eines U-Tales im nördlichen Kaokofeld, Südwestafrika. *Geologische Rundschau*, **46**, 571–575, https://doi.org/10.1007/BF01803042

Morche, D., Schuchardt, A., Dubberke, K. and Baewert, H. 2014. Channel morphodynamics on a small proglacial braid plain (Fagge River, Gepatschferner, Austria). *IAHS-AISH Proceedings and Reports*. Copernicus GmbH, 109–116, https://doi.org/10.5194/piahs-367-109-2015

Nitsche, F.O., Larter, R.D., Gohl, K., Graham, A.G.C. and Kuhn, G. 2016. Crag-and-tail features on the Amundsen Sea continental shelf, West Antarctica. *Geological Society, London, Memoir*, **46**, 199–200, https://doi.org/10.1144/M46.2

Phillips, E.R. 2018. Glacitectonics. *In*: *Past Glacial Environments*. 2nd edn. Elsevier Inc., 467–502, https://doi.org/10.1016/B978-0-08-100524-8.00014-2

Rieu, R., Allen, P.A., Etienne, J.L., Cozzi, A. and Wiechert, U. 2006. A Neoproterozoic glacially influenced basin margin succession and 'atypical' cap carbonate associated with bedrock palaeovalleys, Mirbat area, southern Oman. *Basin Research*, **18**, 471–496, https://doi.org/10.1111/j.1365-2117.2006.00304.x

Roberson, S., Hubbard, B., Coulson, H.R. and Boomer, I. 2011. Physical properties and formation of flutes at a polythermal valley glacier: Midre Lovénbreen, Svalbard. *Geografiska Annaler, Series A: Physical Geography*, **93**, 71–88, https://doi.org/10.1111/j.1468-0459.2011.00420.x

Rose, J. 1991. Subaerial modification of glacier bedforms immediately following ice wastage. *Norsk Geografisk Tidsskrift*, **45**, 143–153, https://doi.org/10.1080/00291959108552267

Sharpe, D.R. 1991. Erosion of bedrock by subglacial meltwater, Georgian Bay, Ontario: a regional view. *Candian Journal of Earth Sciences*, **28**, 623–642, https://doi.org/10.1139/e91-054

Śledź, S., Ewertowski, M.W. and Piekarczyk, J. 2021. Applications of unmanned aerial vehicle (UAV) surveys and Structure from Motion photogrammetry in glacial and periglacial geomorphology. *Geomorphology*, **378**, 107620, https://doi.org/10.1016/j.geomorph.2021.107620

Székely, B., Reinecker, J., Dunkl, I., Frisch, W. and Kuhlemann, J. 2002. *Neotectonic movements and their geomorphic response as reflected in surface parameters and stress patterns in the eastern Alps*. EGU Stephan Mueller Special Publication Series., **3**, 149–166, https://doi.org/10.5194/smsps-3-149-2002

Tedesco, J., Cagliari, J., Coitinho, J., dos Reis Coitinho, J., da Cunha Lopes, R. and Lavina, E.L.C. 2016. Late Paleozoic paleofjord in the southernmost Parana Basin (Brazil): Geomorphology and sedimentary fill. *Geomorphology*, **269**, 203–214, https://doi.org/10.1016/j.geomorph.2016.06.035

van der Vegt, P., Janszen, A. and Moscariello, A. 2012. Tunnel valleys: current knowledge and future perspectives. *In*: Huuse, M., Redfern, J., Le Heron, D.P., Dixon, R.J., Moscariello, A. and Craig, J. (eds) *Glaciogenic Reservoirs and Hydrocarbon Systems*. Geological Society, London, Special Publications, **368**, 75–97, http://dx.doi.org/10.1144/SP368.13

Veh, G., Korup, O. and Walz, A. 2020. Hazard from Himalayan glacier lake outburst floods. *PNAS*, **117**, 907–912, https://doi.org/10.1073/pnas.1914898117

Vehling, L., Baewert, H., Glira, P., Moser, M., Rohn, J. and Morche, D. 2017. Quantification of sediment transport by rockfall and rockslide processes on a proglacial rock slope (Kaunertal, Austria). *Geomorphology*, **287**, 46–57, https://doi.org/10.1016/j.geomorph.2016.10.032

Wyshnytzky, C.E., Lukas, S. and Groves J.W.E. 2020. Multiple mechanisms of minor moraine formation in the Schwarzensteinkees Foreland, Austria. *In*: Waitt, R.B., Thackray, G.D. and Gillespie, A.R. (eds) *Untangling the Quaternary Period: A Legacy of Stephen C. Porter*. Geological Society of America Special Paper, **548**, https://doi.org/10.1130/2020.2548(10)

Zekollari, H., Huss, M. and Farinotti, D. 2019. Modelling the future evolution of glaciers in the European Alps under the EURO-CORDEX RCM ensemble. *The Cryosphere*, **13**, 1125–1146, https://doi.org/10.5194/tc-13-1125-2019